A Hybrid Approach to the Evaluation of Thermal Comfort in Passenger Vehicles

Daniel Gehringer[1,*], Timo Kuthada[2], Andreas Wagner[1]

[1] Institute of Automotive Engineering (IFS), University of Stuttgart
[2] Research Institute for Automotive Engineering and Powertrain Systems Stuttgart (FKFS)
Pfaffenwaldring 12
70569 Stuttgart
* Correspondence: daniel.gehringer@ifs.uni-stuttgart.de

Abstract: Occupant thermal comfort is an important aspect of passenger vehicles. With powertrain electrification and autonomous vehicle operation, interior comfort is gaining increasing importance. The thermal comfort of the cabin must be evaluated during all stages of vehicle development. This study presents a method that enables the digital assessment of thermal comfort during the early development stages using computer-aided design (CAD) geometry of the vehicle, and later in prototypes or production vehicles using a thermal comfort manikin. The thermal comfort manikin equipped with various sensors, along with the corresponding simulation approach, is described. Validation measurements conducted under a controlled environment in a climatic test chamber demonstrate a strong agreement between the measurement and simulation results. Both evaluation methods yield comparable results, thereby allowing for comparisons of measures during different development stages of the vehicle.

1 Introduction

Satisfying the thermal comfort of passengers is an important aspect of modern road vehicles. It influences the overall perceived comfort within a vehicle cabin and, consequently, impacts customers' purchasing decisions. This is especially critical with the growing demand for battery electric vehicles (BEVs), where the energy required to maintain a comfortable interior climate can affect the vehicle's range, making it a decisive factor. Moreover, maintaining occupants in a thermally neutral state also contributes to driving safety [1]. Recent research indicates that thermal sensation can influence the immune levels of the human body [2]. Consequently, thermal comfort within the vehicle cabin must be considered throughout the development process.

One approach to evaluate thermal comfort is through subject trials involving humans. However, conducting such trials during the early stages of development is often

impractical. This can be due to the unavailability of a functional prototype or because the prototype's details are still confidential. In such cases, a standardized process with objective comfort ratings is essential.

The thermal comfort of humans is influenced by various factors, which can be categorized into external factors stemming from the environment and internal factors arising from physiological processes within the human body. Primary environmental influences on thermal comfort include air temperature, the temperature of surrounding surfaces, airflow velocity, and relative humidity [3]. The clothing worn by an individual significantly impacts heat dissipation from the body by acting as an insulating layer against the skin. The metabolic rate accounts for the internal heat generated by metabolic processes within the human body, with the person's activity level predominantly affecting it.

Acclimatization to the ambient climate also plays a role in determining thermal comfort. Research indicates that occupants' expectations concerning indoor climate are influenced by the external climate and their ability to regulate the indoor environment [4]. The external climate largely determines occupants' clothing choices, thus affecting clothing insulation.

This paper will present the development of a thermal comfort manikin (TCM) capable of providing a thermal comfort rating for the entire body, while also assessing factors such as airflow velocity, draught, and temperature on specific body parts. Another aim is to create a digital twin of the manikin that yields comparable results between measurements and simulations. This approach will facilitate a comprehensive evaluation of thermal comfort across all stages of vehicle development. The present work describes the thermal comfort manikin along with its associated software. Experimental measurements are conducted within a climate test chamber to showcase the functionalities of the manikin. The measurement setup is subsequently replicated within a simulation and a comparison between simulation and measurement results is presented.

2 State of the Art

To quantify thermal comfort within an occupied space, it is essential to measure the ambient conditions using appropriate sensors. This encompasses variables such as air temperature, air velocity, relative humidity, and the temperature of surrounding surfaces. Alongside the direct measurement of these parameters, various indices exist to objectively evaluate thermal comfort. Among these is the Predicted Mean Vote (PMV) model, introduced by Fanger [5]. This comfort index is widely used and established in the standard DIN EN ISO 7730 [6] as well as ASHRAE 55 [7]. With its foundation in the principles of heat balance and human physiology, the PMV model calculates an index that represents the average thermal sensation of a group of occupants. It is defined on a scale ranging from -3 to 3, with the corresponding ratings: cold, cool, slightly cool, neutral, slightly warm, warm and hot. An optimal thermal comfort level is attained at a value of 0 on this scale. Its widespread adoption in

research and practice is attributed to its simplicity, applicability, and empirical validation. PMV is defined as

$$PMV = [0.303\, e^{-0.036\, M} + 0.028] \left\{ \begin{array}{c} (M - W) - 3.05 \cdot 10^{-3}[5733 - 6.99(M - W) - p_a] \\ -0.42[(M - W) - 58.15] - 1.7 \cdot 10^{-5} M(5867 - p_a) - 0.0014M(34 - \vartheta_a) \\ -3.96 \cdot 10^{-8} f_{cl}[(\vartheta_{cl} + 273)^4 - (\bar{\vartheta}_r + 273)^4] - f_{cl} h_c(\vartheta_{cl} - \vartheta_a) \end{array} \right\} \quad (1)$$

where M is the metabolic rate, W the external work, p_a the water vapor pressure, ϑ_a the air temperature, f_{cl} the clothing area factor, ϑ_{cl} the clothing temperature, $\bar{\vartheta}_r$ the mean radiant temperature and h_c the convective heat transfer coefficient. Using the PMV value the Projected Percentage of Dissatisfied (PPD) can be calculated as

$$PPD = 100 - 95\, e^{-0.03353\, PMV^4 - 0.2179\, PMV^2}. \quad (2)$$

Details on how each of the parameters used to calculate PMV are obtained with suitable measurement equipment will be described in section 3.1. Figure 1 shows the PMV models scale with all input parameters on the left and the PPD over PMV values according to equation (2).

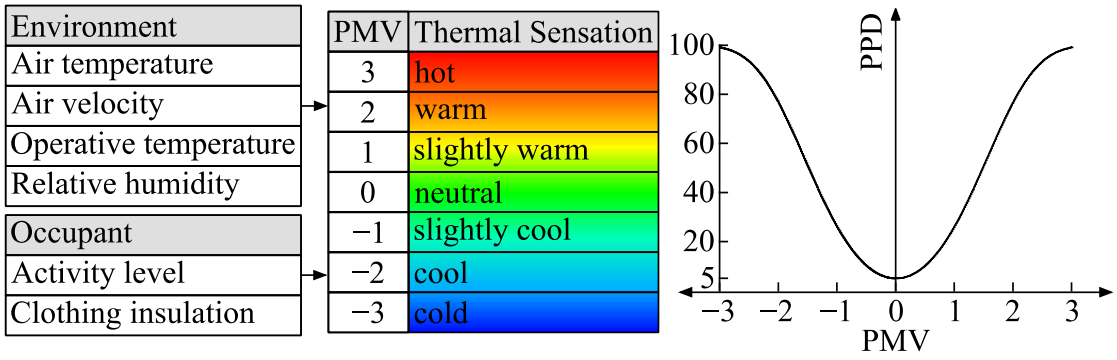

Figure 1: PMV/PPD model scale and its input parameters.

When assessing thermal comfort, it is important to account for the turbulence intensity of the airflow around an occupant. Elevated turbulence levels can result in a sensation of air draught. This can be quantified by the so called draught rate. It describes the percentage of people that would rate a given flow condition as unpleasant due to draught. The draught rate is calculated as

$$DR = \left(34 - \vartheta_{a,l}\right)\left(\bar{v}_{a,l} - 0.05\right)^{0.62}\left(0.37\, \bar{v}_{a,l}\, Tu + 3.14\right), \quad (3)$$

using the local air temperature $\vartheta_{a,l}$, the local mean air velocity $\bar{v}_{a,l}$ and the local turbulence intensity Tu [6]. The Thermal Comfort Manikin calculates this draught rate for the head, neck, chest, hip and lower legs. The turbulence intensity is calculated in percent

$$Tu = \frac{\sigma}{\bar{v}_a}\, 100, \quad (4)$$

where $\bar{v}_a$ is the mean air velocity in the measuring interval and σ the standard deviation of the air velocity

$$\sigma = \sqrt{\frac{1}{n-1}\sum_{i=1}^{n}\left(v_{a,i} - \bar{v}_a\right)^2} \tag{5}$$

using the air velocity at the time i in a measurement interval $v_{a,i}$ [8].

Another source of thermal dissatisfaction in occupant comfort is the presence of a vertical temperature difference in the cabin. The manikin computes the vertical temperature difference $\Delta\vartheta_{a,v}$ between the head and the ankles. With this, the resulting percent dissatisfied for $\Delta\vartheta_{a,v} < 8\,°C$ can be calculated after

$$PD = \frac{100}{1 + e^{5.76 - 0.856\,\Delta\vartheta_{a,v}}} \text{ [6].} \tag{6}$$

The standard DIN 7730 imposes certain limitations on the application of the PMV model under transient ambient conditions. These limitations are categorized into temperature cycles, temperature drifts or drops, and transitions. Peak-to-peak deviations in a temperature cycle that fall below 1 K do not impact the comfort value. Deviations beyond this threshold can lead to reduced comfort. Temperature drifts or drops occurring at rates of change below 2 K/h are considered permissible for using the method. The standard also provides insights into temperature transitions. Immediate effects are observed for significant changes in operative temperature. PMV can be employed to predict comfort when the operative temperature increases. Conversely, when the operative temperature decreases, PMV predicts values that are higher than the perceived thermal sensation. After approximately 30 minutes in stationary conditions, the PMV value becomes applicable once again.

Ekici [9] has shown that the mean radiant temperature significantly affects the calculated PMV values. Some measurement systems take the assumption that the mean radiant temperature is equivalent to the measured air temperature, thus avoiding the need for a separate sensor for mean radiant temperature. However, Chaudhuri et al. [10] showed that this simplification leads to increased uncertainties in PMV predictions. Other studies have indicated that these uncertainties in PMV calculations can be minimized by directly measuring the operative temperature [11]. This can be accomplished using either a globe thermometer or an ellipsoid-shaped probe.

The diameter of a globe thermometer primarily impacts the uncertainty of the measured mean radiant temperature [12], and the use of globe thermometers can introduce significant systematic errors [13,14]. ISO 7726 [8] states that an ellipsoid sensor is more suitable and provides design specifications for an operative temperature probe. In research conducted by Simone et al. [15], which compared various operative temperature sensor types, an ellipsoid-shaped sensor was employed as a reference. The study also concluded that a black sensor tends to overestimate the influence of short-wave radiation, while a white or reflective sensor tends to underestimate it. As a result, the use of a flat gray sensor color is recommended [15], aligning with the specifications in ISO 7726 [8]. An ellipsoid-shaped sensor offers a

projected area factor that better corresponds to that of a human, affecting the relationship between convection and radiation heat transfer on the sensor.

The metabolic rate and clothing factor exert a significant influence on the PMV value. The calculated PMV index becomes more sensitive to the mean radiant temperature during light metabolic rates. Conversely, at higher metabolic rates, the impact of other parameters diminishes [16]. Tables to determine the activity level and clothing index are available in the standards ISO 7730 [6] and ASHREA 55 [7] for example.

3 Methodology

This chapter will highlight the technical background of the developed thermal comfort manikin. Firstly, the hardware manikin buildup, sensor equipment, and measurement software are described. A corresponding simulation approach with a digital twin of the TCM is presented in the second section of this chapter.

3.1 Thermal Comfort Manikin

The manikin's geometry is derived from that of a 50^{th} percentile western male human, with a total height of 1.78 m [17,18]. The base frame comprises 30 x 30 mm aluminum profiles connected by various joints. These joints allow for the adaptation of the manikin to different body positions. The potential degrees of freedom for each joint are outlined in Table 1. All exterior shell components of the manikin are manufactured using a fused deposition modeling (FDM) printer. The outer shell parts include apertures for sensor mounting and slots for routing cables through the manikin.

Table 1: Degrees of freedom of base frame joints.

	Joint Type	Range of Motion in °
Neck	Revolute	±10
Shoulder	Ball	180
Lower Torso	Revolute	±5
Hips	Revolute	90
Elbows	Revolute	90
Knee	Revolute	90

Sensors are incorporated into the external shell of the manikin. The measurement system comprises four distinct sensor types: eight air velocity and temperature probes, one operative temperature probe, 32 thermocouples, and one relative humidity probe. The placement of the probes is determined based on the distribution of thermoreceptors on the human body. Thermoreceptors enable humans to perceive alterations in skin temperature [3]. Locations with a high concentration of

thermoreceptors are selected for sensor placement. Figure 2 shows the thermoreceptor density on the human skin and the chosen sensor positions for the manikin.

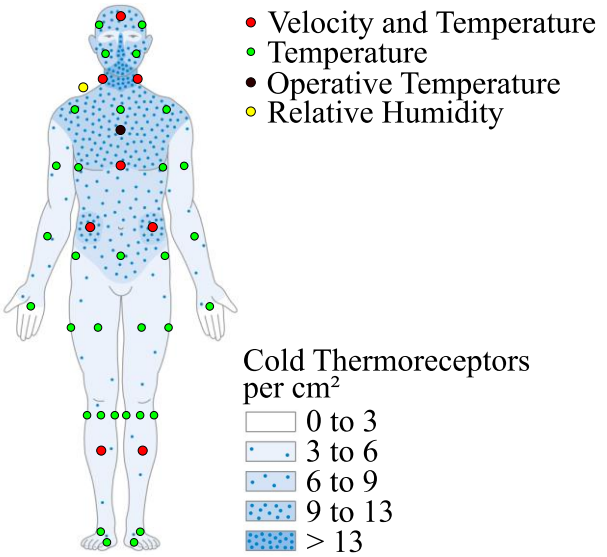

Figure 2: Thermoreceptor density on the human body and sensor placement, based on [3].

The velocity probes are mounted to a laser-cut steel plate, which is fastened to the outer shell of the manikin. Steel cages are positioned over the probes to shield them during handling, minimally obstructing airflow to the sensing surfaces. Thermo-couples are affixed to small carbon tubes within the shell. This arrangement allows for protective covers to be added when transporting or handling the manikin.

The operative temperature probe is a gray ellipsoid measuring 156 mm in length and 55 mm in diameter. The sensor's surface is influenced by both convection and radiation, possessing an emissivity coefficient of 0.95. Various body postures can be simulated by adjusting the sensor angle. The ellipsoidal shape ensures that the projected area ratio on the surrounding surfaces matches that of a human body. For instance, a standing individual is simulated with an upright orientation, while a seated person is represented at a 30° angle between the floor and the sensor. Horizontally positioning the sensor models a person lying down [8]. Employing such an operative temperature probe can reduce uncertainties in PMV calculation when compared to individual measurements of air temperature and mean radiant temperature. The probe's uncertainty is required to be below 0.2 °C [11]. The probe utilized in the manikin achieves this level of accuracy within the temperature range of 10 to 40 °C [19]. Figure 3 shows the TCM on a vehicle seat with all sensors attached.

Figure 3: Thermal comfort manikin with sensors on a vehicle seat.

A LabVIEW program featuring a graphical user interface (GUI) was developed for the purpose of acquiring measurement data. LabVIEW is a software package that employs a visual programming language, designed by National Instruments. Within the program, measurement signals undergo processing to reach their final format, and additional values are computed. The resulting measurement file encompasses all sensor measurements alongside the computed comfort evaluation parameters. The program allows real-time display of both measurement and comfort values, thereby enabling the assessment of the effects of configuration changes during a measurement session. The sensors allow for ambient pressure and humidity correction of flow velocity measurements. These corrections can be enabled in the measurement program. The measured humidity values of the manikin's sensor is directly used. Pressure values must be specified through the GUI.

Physical quantities measured by the comfort manikin include flow velocity v_a, air temperature ϑ_a, operative temperature ϑ_o and relative humidity φ. The proposed measurement manikin enables the assessment of thermal comfort through direct interpretation of sensor data or via computed comfort values. The sensor data can be employed for comparing different setups or vehicles. While interpreting the measurement results requires expertise in the field, additional comfort values are subsequently derived due to the challenging nature of directly interpreting these measured values.

The instrumentation used on the TCM measures the operative temperature. It describes the temperature of an imaginary black enclosure where the human would exchange the same amount of heat due to radiation and convection as in the measured environment. For the computation of the PMV, the mean radiant temperature becomes necessary. It is defined in a manner analogous to the operative temperature, but only takes into account the heat exchange due to radiation excluding convection. The mean radiant temperature is calculated as

$$\bar{\vartheta_r} = \sqrt[4]{(273.15 + \vartheta_o)^4 + \frac{h_{c,o}}{\varepsilon_o\, \sigma}(\vartheta_o - \vartheta_a)} - 273.15, \tag{7}$$

using the measured operative temperature ϑ_o, air temperature ϑ_a, Stefan-Boltzmann constant σ, emission coefficient of the operative temperature probe ε_o and the convective heat transfer coefficient

$$h_{c,o} = \max\left(18\ {v_a}^{0.55}, 3\ \sqrt[4]{|\vartheta_o - \vartheta_a|}\right). \quad (8)$$

The correlation calculates the convective heat transfer coefficient for both forced and free convection, selecting the higher value for the computation of the mean radiant temperature.

3.2 Simulation Approach

To allow thermal comfort prediction during the early development process when no prototype is available, a simulation approach is required. Results should be comparable to the measurement results conducted with the thermal comfort manikin. This comparability enables the validation of simulation models employed in the development process, possibly with the final prototype. For the computational fluid dynamics (CFD) simulation, Dassault Systèmes' PowerFLOW software package with its Lattice-Boltzmann Method (LBM) based solver is employed. The proposed simulation workflow comprises five distinct steps, outlined in Figure 4. The discretized manikin model can be positioned in the cabin with the pre-processing tool ANSA. The model is set up as a LS-DYNA dummy, which allows translation of the digital manikin and articulation of the joints in accordance with the degrees of freedom of the hardware manikin. Sensors are modeled as rigid body nodes connected to the surface mesh of the manikin. The resulting Nastran file is processed using a python script to extract sensor positions, which are then compiled into a text file containing all necessary probe data. This text file can be seamlessly imported into PowerFLOW by the python script. This script automates the generation of fluid and surface measurement probes at the relevant locations within the CFD model. Following the simulation run, results for all probe locations can be exported using a post-processing script. This script employs the PowerACOUSTICS software to extract the results and transfers the resultant text files to an output directory. These text files contain all physical quantities described earlier. In the final step, the output files are read by the LabVIEW program, which computes the thermal comfort values and outputs these values to a TDMS file. The structure of this output file replicates that of the measurement files generated through thermal comfort dummy measurements.

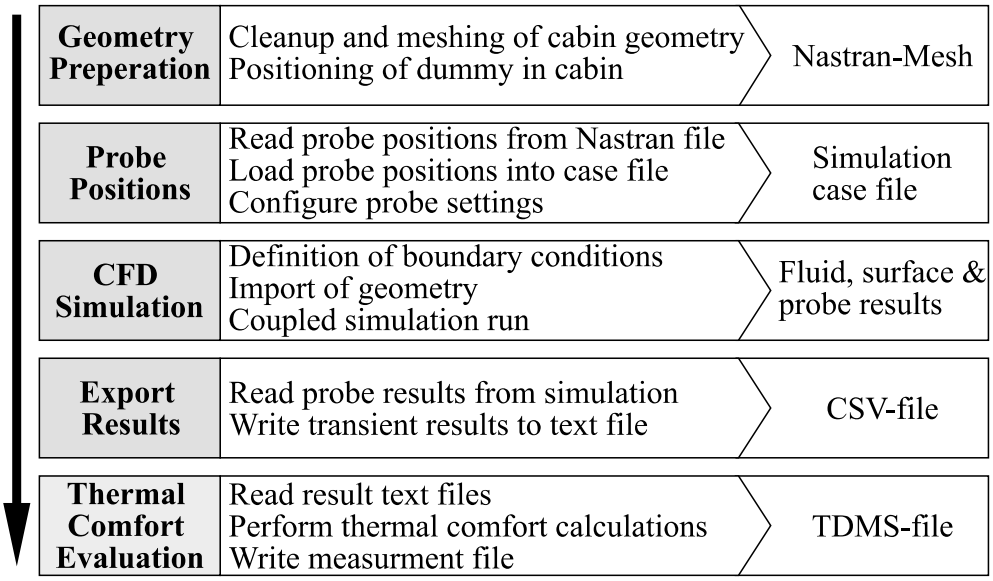

Figure 4: Thermal Comfort Manikin simulation workflow.

Velocity, humidity sensors and thermocouples are modeled as probes without geometry in the CFD simulation. However, the operative temperature probes' geometry is discretized. This is necessary to incorporate radiation effects on the sensor surface, which in turn impact the measured temperature. The temperatures of all surface nodes of the operative temperature sensor are exported to the result file. Subsequently, in the LabVIEW evaluation program, these temperatures are averaged, defining the operative temperature.

To simulate heat-up or cool-down cases spanning over several minutes, a computationally efficient transient approach is needed. Such cases require distinct methods and entail some simplifying assumptions. In case of transient heat up or cool down measurements, an initial flow development simulation is followed with a velocity freeze simulation [20]. The first 3 to 10 seconds are simulated to establish the flow field within the cabin. During this transient simulation, the draught rates and comfort values are calculated using the result data of the fluid file. In the subsequent step, the averaged flow field obtained from the first simulation is frozen. The computational grid is coarsened, and only the surface and fluid temperatures are simulated, while all other flow parameters are kept constant. The humidity can vary during this simulation step. If there are changes in the inlet mass flow rate, further flow development simulations are run. Subsequently, another velocity freeze simulation ensues at the new mass flow rate, as illustrated in Figure 5.

During velocity freeze simulations, where the velocity field is held constant, the air velocity remains unchanged over time. As a consequence, calculating the turbulence intensity and draught rate becomes impractical. In these scenarios, a workaround is implemented: the turbulence intensity and mean air velocity from the previous flow development simulation are averaged over time and treated as constants throughout the simulation cycle. This, combined with the evolution of air temperature, allows for the computation of the draught rate in accordance with equation (3).

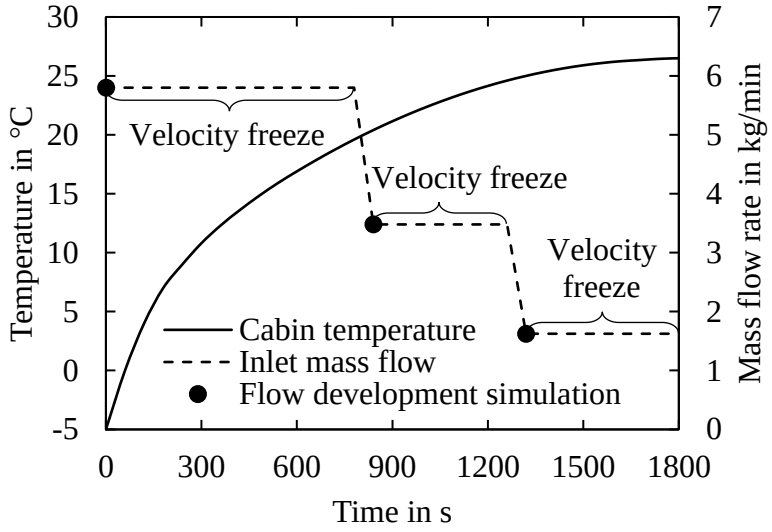

Figure 5: Simulation approach for transient heat up cases.

During transient simulations, accurate modeling of the manikin's specific heat capacity is crucial for achieving realistic temperature changes over time. To streamline the simulation process, a single specific heat capacity value $c_{p,manikin}$ is calculated for the manikin. This calculation employs a mass-weighted average method, incorporating the individual materials' mass m_i and their respective specific heat capacities $c_{p,i}$, as well as the overall mass of the manikin $m_{manikin}$:

$$c_{p,manikin} = \frac{1}{m_{manikin}} \sum_{i=1}^{n} m_i c_{p,i}. \tag{9}$$

3.3 Experimental Setup

Measurements were conducted in a climate test chamber to validate the presented approach. The specific chamber used was the Weiss Umwelttechnik GmbH WT 8'/40-60, with a usable interior space of 2 x 2 x 2 m. This chamber offers a temperature range of -30 to 60 °C, with a heating and cooling rate of 1 K per minute and a time consistency of ≤ ± 1 K. Utilizing a climate test chamber guarantees a controlled environment with well-defined boundary conditions. A box is positioned in the climate test chamber, it can be supplied with a controlled airflow through a connected pipe with integrated fan. This pipe is supplied directly with air from the climate chamber conditioning system, which houses both air heater and evaporator. The box has an interior volume of 1.25 m³; which corresponds to the interior volume per person typically found in autonomous people mover concepts [21,22]. Due to this correspondence, it is referred to as "ThermoCab" in the subsequent discussion. To simulate a heated wall and account for the influence of uneven wall temperatures on the mean radiant temperature, a heating foil with a total power output of 190 W is

affixed to the interior rear wall. The comfort manikin is positioned on a chair in the center of the ThermoCab in a seated position. The operative temperature probe angle is set to 30° to represent a seated human. Stationary measurements over 30 seconds at different temperature levels with isothermal air injection were conducted. Each measurement was preceded by a soak duration of at least one hour to ensure stable and uniform temperature distribution, thus adhering to the requirements for consistent ambient conditions as outlined in EN ISO 7730 [6]. To assess the reproducibility of the results, all measurements were repeated three times. Clothing values were adjusted to match the ambient temperature conditions, aiming to achieve a PMV value close to neutral. The metabolism value was maintained constant at 1.1 to represent a seated individual.

The measurement setup is modeled using the simulation workflow described in section 3.2. The experiment is shown in the left and the corresponding simulation model in the right side of Figure 6. Radiation has a large influence on the operative temperature probe. Consequently, accurately modeling the radiation effect in the simulation becomes crucial. Apart from its absolute surface temperature T and surface area A, the Stefan-Bolzmann constant σ, as well as the thermal emissivity ε of a body determines its radiative heat flow

$$\dot{Q} = \varepsilon \, \sigma \, A \, T^4. \tag{10}$$

Figure 6: Climate chamber measurement setup (left) and simulation model (right).

The thermal emissivity values for both the interior walls of the test chamber, ThermoCab and the surface of the manikin were measured and incorporated into the simulation setup. A hand-held measurement device (Inglas TIR 100-2) that employs the total internal reflection (TIR) principle, as described in DIN EN 15976 and 16012 [23,24], was used to measure the thermal emissivity. It has a measurement range of 0.02 to 0.98, a repeatability accuracy of ± 0.005 for low and ± 0.01 for high emissivity specimens [25,26]. All interior measurements within the test chamber were integrated

into the simulation. The temperatures of the ThermoCab walls were monitored throughout all tests. These measured temperatures are used as prescribed boundary conditions within the simulation. Further, the mass flow rate, temperature and humidity of the supply air into the ThermoCab are also recorded during the measurement.

4 Results

In the following, a heat-up case from 5 to 30 °C is presented. The Climate chamber, including the ThermoCab and manikin, was pre conditioned to 5 °C. At measurement start, the inlet mass flow rate was set to 2.11 kg/s, with the inlet temperature gradually rising to 30 °C over the course of 60 minutes. Figure 7 illustrates the measurement data collected at the ThermoCab inlet during this heat-up process. To promote a more uniform vertical temperature distribution due to natural convection and buoyancy caused by the injection of warmer air into the ThermoCab, the air outlets were oriented downward at a 45° angle.

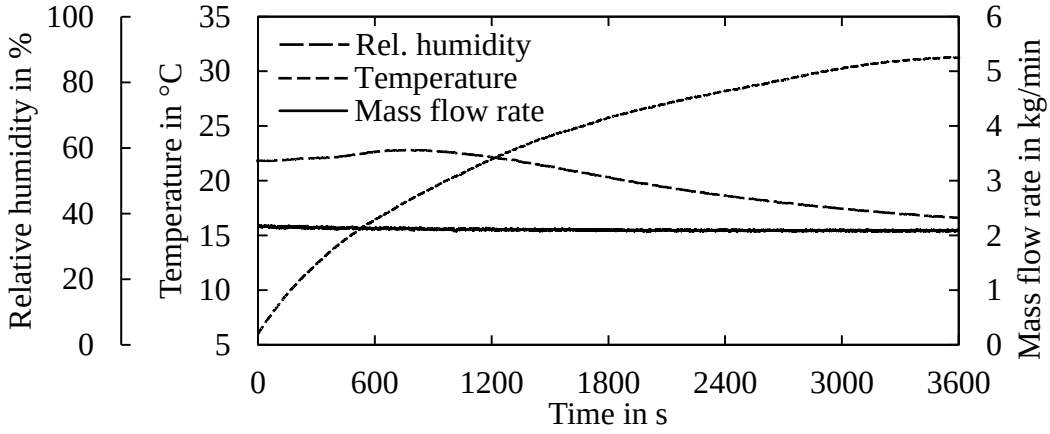

Figure 7: Measured inlet conditions of heat-up case.

Because the inlet mass flow rate remained approximately constant, only one cycle of flow development, followed by a velocity freeze simulation, was used. The flow development simulation was run for 10 seconds. The fluid domain was initialized with a flow velocity of 0 and a temperature of 5.5 °C, corresponding to the measured values. Inlet boundary conditions, including the inlet mass flow rate, temperature, and humidity, were derived from the measurements. Figure 8 depicts a y-aligned velocity cross-section positioned in the middle of the right air outlet after 10 seconds of simulation time. The flow has fully developed throughout the entire ThermoCab.

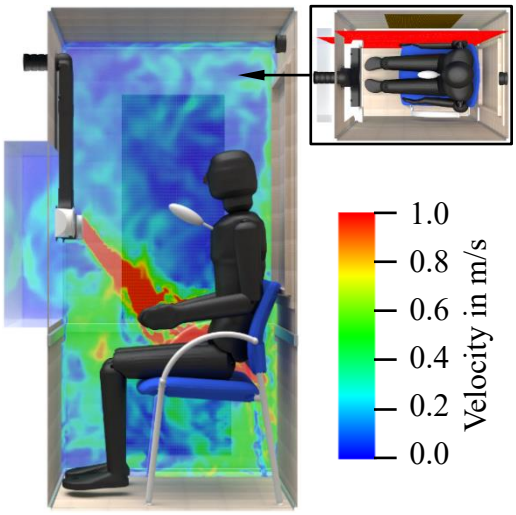

Figure 8: Y-aligned slice of the developed flow inside the ThermoCab.

In Figure 9, the flow velocities during the initial 10 seconds are compared to the measurement values over time for each probe. The comparison of probe data reveals a strong agreement between the measurement and simulation results. Specifically, for the left abdomen probe, the simulation shows slightly higher values in comparison to the measured data. Conversely, both lower leg probes exhibit slightly lower values in the simulation results. To facilitate this comparison further, Table 2 presents additional calculated statistical values for the air velocities. The table compares mean velocities, standard deviations σ, turbulence intensity Tu, and draught rate DR for each probe. Once again, these values indicate a good correlation, with the left abdomen probe exhibiting slightly higher mean and maximum values, while the lower leg probes show lower mean and maximum values when compared to the measurements. The protective cage fitted to the probes on the manikin can potentially influence the incident flow and introduce some turbulence. However, in the simulation, this cage is not modeled, which could lead to discrepancies in the results.

The air temperature values from all probes on the manikin exhibit a root mean square error (RMSE) of 0.8 K or less during the flow development simulation. Consequently, these values are not presented in detail here. The operative temperature, averaged over the 10-second interval, is 5.4 °C in both experiment and simulation. The transient temperature evolution leads to a RMSE of 0.1 K. The average relative humidity in the measurement is 52.3 %, compared to 50.4 % in the simulation, or a RMSE of 2.0 % between the two datasets.

Following the ten-second flow development simulation, the fluid domain is averaged over the last second of simulation time. This averaged flow field serves as the initial condition for the subsequent velocity freeze simulation. During this phase, velocities do not vary over time, and only the temperature evolution within the fluid domain is computed through the coupled simulation with a coarsened mesh, as outlined in section 3.2.

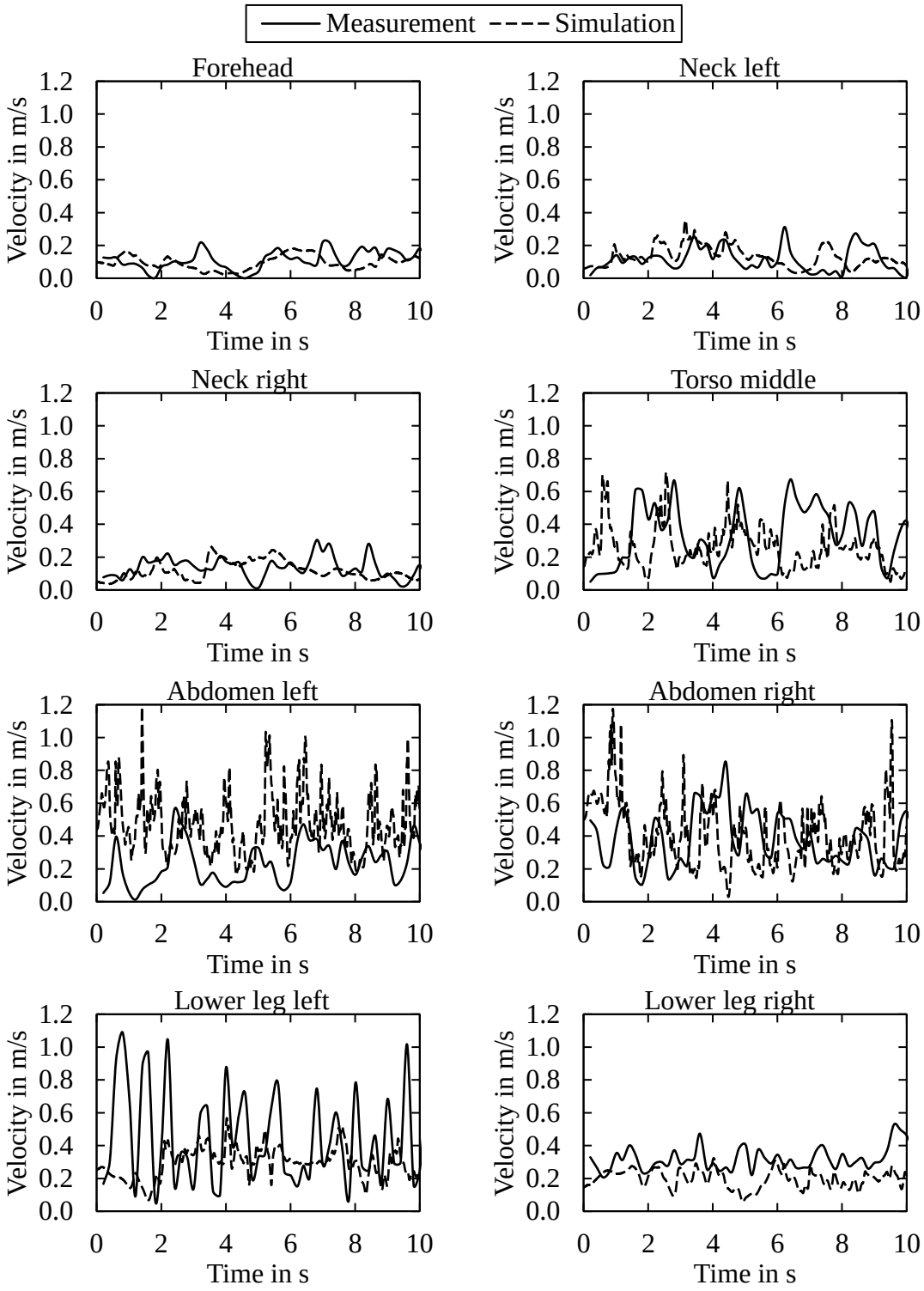

Figure 9: Comparison of velocity probe data between measurement and simulation.

Table 2: Statistical comparison of velocities between measurement and simulation.

	Measurement				Simulation			
	$\bar{v}_a$ m/s	σ m/s	Tu %	DR %	$\bar{v}_a$ m/s	σ m/s	Tu %	DR %
Forehead	0.11	0.06	49.5	26.6	0.10	0.04	44.6	19.8
Neck left	0.12	0.07	63.2	30.1	0.13	0.06	47.4	33.0
Neck right	0.14	0.06	47.0	34.1	0.12	0.06	46.4	28.2
Torso middle	0.33	0.19	56.2	100.0	0.26	0.13	48.9	83.9
Abdomen left	0.23	0.13	56.6	79.1	0.47	0.18	37.2	100.0
Abdomen right	0.39	0.17	43.6	100.0	0.41	0.19	47.9	100.0
Lower leg left	0.45	0.29	65.6	100.0	0.30	0.09	31.1	78.2
Lower leg right	0.32	0.07	22.2	73.7	0.20	0.05	27.2	44.6

A comparison of PMV values derived from measurement and simulation of the heat-up case is illustrated in Figure 10. In the simulation, surface temperatures are updated after every coupling interval between the CFD and thermal solver. Since surface temperatures have a direct impact on the operative temperature, the PMV is calculated at the same interval when the surface temperatures are updated. The comfort value obtained from measurements exhibits slight fluctuations due to changes in flow velocity. Initially, when average air and surface temperatures are below 6 °C, the PMV value in both measurement and simulation is -3. However, as the air and surface temperatures within the ThermoCab increase, the PMV value also rises. A neutral thermal state, represented by a PMV of 0, is attained after 2984 seconds in the experiment and 3060 seconds in simulation.

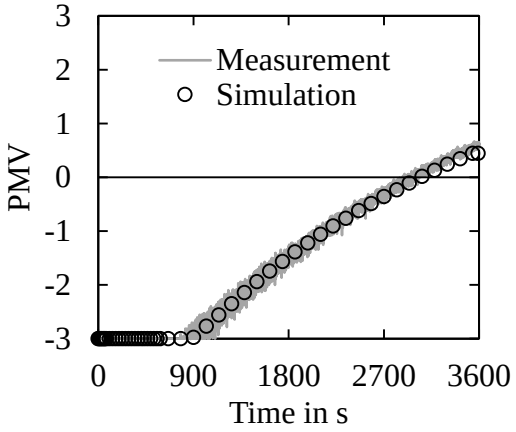

Figure 10: Comparison of calculated PMV values for heat-up case.

The air temperature averages over all probes at the end of the heat-up cycle (t=3600 s) is only 0.9 K higher in the simulation results. This deviation lies within the measurement accuracy of the thermocouples used in the TCM.

5 Conclusions and Outlook

The proposed thermal comfort manikin enables the measurement and real-time examination of velocity and temperature fields within a vehicle cabin. It takes radiation as well as relative humidity into account. Together with the clothing and metabolism factors defined in the measurement GUI, an objective rating of the thermal comfort is possible. The simulation approach presented, utilizing a digital twin of the TCM, provides results that are comparable to measurements. Both the velocity field obtained from the initial flow development simulations and the temperature evolution over time derived from subsequent frozen velocity field simulations as well as the calculated PMV align well with measurement values.

In the future, an approach to weigh temperatures and velocities at different locations of the body according to the thermal sensitivity of the body part will be implemented into the software. This enhancement will enable a more precise evaluation of temperature distributions across the body, recognizing that not all regions contribute equally to the overall thermal sensation. Furthermore, the TCM will be applied to a vehicle cabin, and its results will be compared to those obtained from other comfort models in simulations.

6 Acknowledgements

This research is accomplished within the project “UNICARagil” (FKZ 16EMO0289). We acknowledge the financial support for the project by the Federal Ministry of Education and Research of Germany (BMBF).

7 Abbreviations

BEV	Battery Electric Vehicle
CAD	Computer-Aided Design
CFD	Computational Fluid Dynamics
FDM	Fused Deposition Modeling
GUI	Graphical User Interface
LBM	Lattice-Boltzmann Method
PMV	Predicted Mean Vote
PPD	Projected Percentage of Dissatisfied
TCM	Thermal Comfort Manikin
TIR	Total Internal Reflection

8 Bibliography

1. Daanen, H. A.M.; van de Vliert, E.; Huang, X.: Driving performance in cold, warm, and thermoneutral environments. Applied Ergonomics 34 (2003), p. 597-602.
2. Cheng, X.; Zhou, Z.; Yang, C.; Zheng, X.; Liu, C.; Huang, W.; Yang, Z.; Qian, H.: Effects of draught on thermal comfort and respiratory immunity. Building and Environment 224 (2022), p. 109537.
3. Brandes, R.; Lang, F.; Schmidt, R. F.: Physiologie des Menschen: mit Pathophysiologie, Springer Lehrbuch, 32. Auflage, Berlin, Heidelberg: Springer, 2019.
4. Brager, G. S. u. Dear, R. J. de: Thermal adaptation in the built environment: a literature review. Energy and Buildings 27 (1998) 1, p. 83–96.
5. Fanger, P. O.: Thermal comfort analysis and applications in environmental engineering. Analysis and applications in environmental engineering. New York: McGraw-Hill, 1970.
6. Deutsches Institut für Normung e.V.: DIN EN ISO 7730:2006-05, Ergonomie der thermischen Umgebung – Analytische Bestimmung und Interpretation der thermischen Behaglichkeit durch Berechnung des PMV- und des PPD-Indexes und Kriterien der lokalen thermischen Behaglichkeit. Berlin: Beuth Verlag GmbH, 2006.
7. American Society of Heating, Refrigerating and Air-Conditioning Engineers: ANSI/ASHRAE Standard 55-2017: Thermal Environmental Conditions for Human Occupancy. Atlanta: ASHRAE, 2017.
8. Deutsches Institut für Normung e.V.: DIN EN ISO 7726:2021-03, Umgebungsklima - Instrumente zur Messung physikalischer Größen. Deutsche Norm. Berlin: Beuth Verlag GmbH, 2021.
9. Ekici, C.: Measurement Uncertainty Budget of the PMV Thermal Comfort Equation. International Journal of Thermophysics 37, Issue 5, 2016.
10. Chaudhuri, T.; Soh, Y. C.; Bose, S.; Xie, L.; Li, H.: On assuming Mean Radiant Temperature equal to air temperature during PMV-based thermal comfort study in air-conditioned buildings. IECON 2016 - 42nd Annual Conference of the IEEE Industrial Electronics Society. IEEE 2016, p. 7065–7070.
11. Broday, E. E.; Ruivo, C. R.; Gameiro da Silva, M.: The use of Monte Carlo method to assess the uncertainty of thermal comfort indices PMV and PPD: Benefits of using a measuring set with an operative temperature probe. Journal of Building Engineering 35 (2021) 4, p. 101961.
12. Da Silva, M. G.; Santana, M. M.; Alves e Sousa, J.: Uncertainty Analysis of the Mean Radiant Temperature Measurement based on Globe Temperature Probes. Journal of Physics: Conference Series 1065 (2018), p. 72036.

13. Teitelbaum, E.; Chen, K. W.; Meggers, F.; Guo, H.; Houchois, N.; Pantelic, J.; Rysanek, A.: Globe thermometer free convection error potentials. Scientific reports 10 (2020) 1, p. 2652.
14. Teitelbaum, E.; Alsaad, H.; Aviv, D.; Kim, A.; Voelker, C.; Meggers, F.; Pantelic, J.: Addressing a systematic error correcting for free and mixed convection when measuring mean radiant temperature with globe thermometers. Scientific reports 12 (2022) 1, p. 6473.
15. Simone, A; Babiak, J.; Bullo, M.; Landkilde, G.; Olesen, B. W.: Operative temperature control of radiant surface heating and cooling systems. In: Proceedings of Clima 2007 Wellbeing Indoors.
16. Dyvia, H. A.; Arif, C.: Analysis of thermal comfort with predicted mean vote (PMV) index using artificial neural network. IOP Conference Series: Earth and Environmental Science 622, 2021, p. 12019.
17. Deutsches Institut für Normung e.V.: DIN EN ISO 7250-1:2017-12, Wesentliche Maße des menschlichen Körpers für die technische Gestaltung – Teil 1: Körpermaßdefinitionen und –messpunkte. Berlin: Beuth Verlag GmbH, 2017.
18. Deutsches Institut für Normung e.V.: DIN CEN ISO/TR 7250-2:2013-08, Wesentliche Maße des menschlichen Körpers für die technische Gestaltung – Teil 2: Anthropometrische Datenbanken einzelner nationaler Bevölkerungen. Berlin: Beuth Verlag GmbH, 2013.
19. Dantec Dynamics A/S: ComfortSense – Installation and User Guide. Publication No.: 9040U4652, Skovlunde, 2016.
20. Dassault Systèmes: PowerFLOW – Climate Control Best Practices Guide PF5.5BP, DS Simulia, 2019.
21. Wisser, M.: Konstruktion einer generischen und anpassbaren Peoplemover-Kabine zur Simulation verschiedener Klimatisierungkonzepte. Masterarbeit, Universität Stuttgart, 2022.
22. Gehringer, D.; Kuthada, T.; Wagner, A. Thermal Management System of the UNICARagil Vehicles—A Comprehensive Overview. World Electr. Veh. J. 2023, 14, 6.
23. Deutsches Institut für Normung e.V.: DIN EN 15976:2011-07, Abdichtungsbahnen – Bestimmung des Emissionsgrades. Berlin: Beuth Verlag GmbH, 2011.
24. Deutsches Institut für Normung e.V.: DIN EN 16012:2015-05, Wärmedämmstoffe für Gebäude – Reflektierende Wärmedämm-Produkte – Bestimmung der Nennwerte der wärmetechnischen Eigenschaften. Berlin: Beuth Verlag GmbH, 2015.
25. INGLAS GmbH & Co. KG: TIR 100-2: Measuring of thermal emissivity within seconds. Stand 2/2010.
26. Kononogova, E.; Adibekyan, A.; Monte, C.; Hollandt, J.: Characterization, calibration and validation of an industrial emissometer. Journal of Sensors and Sensor Systems 8 (2019) 1, p. 233–242.